Anharmonic, Temperature, and Matrix Effects on the Molecular Structure and Vibrational Frequencies of Lanthanide Trihalides LnX_3 (Ln = La, Lu; X = F, Cl)

Giuseppe Lanza* and Camilla Minichino

Dipartimento di Chimica, Università della Basilicata, via Nazario Sauro 85, 85100 Potenza, Italy

Received: September 14, 2004; In Final Form: November 30, 2004

MP2 and CCSD(T) ab initio calculations have been carried out to elucidate geometrical structure and vibrational frequencies of representative lanthanide trihalides LnX_3 (Ln = La, Lu; X = F, Cl) explicitly including temperature, anharmonic, inert-gas matrix, and spin−orbit effects. The results have been compared with gas-phase electron diffraction, gas-phase IR measurements, and IR spectra of molecules trapped in inert-gas matrices. On the Born−Oppenheimer surface $LaCl_3$, LuF_3, and $LuCl_3$ adopt trigonal planar (D_{3h}) geometry while LaF_3 assumes a slightly pyramidal (C_{3v}) structure. Because of normal-mode anharmonicities, the resulting thermal average bond angles are considerably lower than the equilibrium ones, while vibrationally averaged bond lengths are predicted to be longer. The inert-gas matrix effects, modeled by the coordination of two inert-gas molecules $LnX_3 \cdot IG_2$ (IG = Ne, Ar, Xe, and N_2), are substantial and strongly depend on the polarizability of coordinating particles. Coordinating inert-gas units always favor the tendency of LnX_3 molecules to adopt planar structure and induce noticeable frequency shifts.

Introduction

The molecular properties of simple monomeric lanthanide trihalides are of significant importance and have been examined extensively by both experimentalists and theoreticians over the past decades.[1,2] The elucidation of the geometry, vibrational motions, and electronic structure is an essential prerequisite to understand their basic chemical properties. Major experimental efforts have been carried out using the electron diffraction (ED) technique[3−5] and vibrational spectroscopies (mainly IR measurements)[6−13] to derive geometry and vibrational frequencies, while electronic structure information has been derived from gas-phase photoelectron spectroscopy.[14] These studies provided very important reference data even though their interpretation is not likely to provide a comprehensive and unbiased view of lanthanide molecular properties. These uncertainties are mainly due to the very high temperature (>1000 K) required for gas-phase measurements[1] and to the host−guest interactions occurring in inert-gas matrices.[15] On the other hand, recent advances in quantum chemistry have provided a complementary and independent tool to probe molecular properties of lanthanide halides,[16−27] and a synergistic experimental/theoretical analysis seems to be particularly fruitful.

In a recent theoretical ab initio study on structure and vibrational frequencies of the GdX_3 (X = F, Cl) molecules we showed that very important spectral features can be interpreted only by explicitly including anharmonicity, temperature and inert-gas matrix effects.[28,29] On this basis a comprehensive and accurate theoretical study on LnX_3 molecules requires approaches that go beyond the standard quantum chemical calculations, and the inclusion of the above-mentioned effects is mandatory.[28,29]

This contribution extends our previous ab initio analysis on the GdX_3 molecules to other lanthanide trihalides, namely, LaX_3 and LuX_3, which are representative elements along the lanthanide series. Thus, we have gathered information on halides of the first (La, $4f^0$), the middle (Gd, $4f^7$), and the last (Lu, $4f^{14}$) elements of lanthanide series to probe in a systematic manner the effect of lanthanide contraction on molecular properties. For such molecules, the symmetric occupation of the 4f shell (empty, half-filled, and filled) prevents significant relativistic spin−orbit coupling for the ground state, thus allowing the inclusion of high-order correlation effects and the use of extended basis sets within a single-component wave function. The fluoride/chloride structure comparison for various lanthanide elements is also particularly interesting. In fact, both fluorides and chlorides are characterized by very shallow out-of-plane bending potentials and, depending on the metal, equilibrium structure changes from slightly pyramidal → quasi-planar → planar. Therefore, the molecules under analysis show a variety of intriguing potential energy curves along the large-amplitude out-of-plane motion.

Computational Details

Electronic Structure Calculations. The relativistic effective core potentials of Stevens et al.[30] that explicitly treat semicore 5s and 5p and valence 4f electrons were used for the lanthanum and lutetium atoms. RECP for the xenon atom was also adopted to describe core electrons while valence electrons were described by a [41,41] basis set contraction.[31] An extra "sp" function ($\alpha = 0.06$) was added to the xenon basis set to warrant compatibility and comparability with results obtained for other inert-gas atoms. The Huzinaga all-electron (10s,6p) and (12s,9p) basis sets contracted as [62111,411] by Dunning[32] and as [631111,52111] by McLean et al.[33] were adopted for first- and for second-row atoms, respectively. These basis sets were complemented with two "d" polarization functions and are hereafter indicated as TZ2D (N $\alpha_1 = 1.60$, $\alpha_2 = 0.40$; F $\alpha_1 = 1.976$, $\alpha_2 = 0.425$; Ne $\alpha_1 = 1.90$, $\alpha_2 = 0.475$; Cl $\alpha_1 = 1.96$, $\alpha_2 = 0.36$; Ar $\alpha_1 = 1.70$, $\alpha_2 = 0.425$; Xe $\alpha_1 = 1.60$, $\alpha_2 = 0.40$). Recently, we showed that very large basis sets for both halogens and gadolinium are required to obtain converged bond lengths for the GdF_3 and $GdCl_3$ molecules.[29] Therefore, some calculations were performed adding two "g" polarization

10.1021/jp045843h CCC: $30.25
Published on Web 02/18/2005

TABLE 1: Calculated Equilibrium Bond Lengths R_e, Bond Angles Θ_e, Harmonic Vibrational Frequencies, and IR Intensities of Isolated LnX_3 Molecules

				ν_1		ν_2		ν_3		ν_4	
	computational level	R_e Å	Θ_e deg	ω cm^{-1}	IR km mol^{-1}	ω cm^{-1}	IR km mol^{-1}	ω cm^{-1}	IR km mol^{-1}	ω cm^{-1}	IR km mol^{-1}
LaF_3	TZ2D/RHF	2.169	120	523.4	0.0	10.0	94.9	514.8	256.2	125.9	24.8
	TZ2D/MP2	2.169	117.6	524.3	8.8	44.9	75.6	516.3	230.4	120.9	18.6
	TZ2D/CCSD(T)	2.169	117.7								
	TZ2D2G2F+/MP2-AE[a]	2.158	116.2	530.5	14.1	53.8	70.6	517.9	234.2	123.9	17.1
LuF_3	TZ2D/RHF	1.984	120	596.0	0.0	58.6	97.4	584.3	187.3	145.8	25.9
	TZ2D/MP2	1.966	119.7	594.8	0.7	20.1	83.3	585.2	171.8	149.6	18.0
	TZ2D/CCSD(T)	1.974	120								
	TZ2D2G2F+/MP2-AE[a]	1.971	120	590.2	0.0	24.1	81.9	580.2	174.7	139.7	17.5
$LaCl_3$	TZ2D/RHF	2.652	120	305.9	0.0	31.8	48.4	325.1	157.8	71.7	8.6
	TZ2D/MP2	2.623	120	311.8	0.0	1.9	41.5	337.0	145.8	68.8	6.0
	TZ2D/CCSD(T)	2.632	120								
	TZ2D2G2F+/MP2-AE[a]	2.603	120	315.4	0.0	3.1	39.3	341.4	144.2	67.2	5.3
$LuCl_3$	TZ2D/RHF	2.439	120	335.8	0.0	54.0	40.7	353.4	111.2	82.9	8.2
	TZ2D/MP2	2.397	120	341.6	0.0	42.1	34.5	364.4	99.9	80.7	5.1
	TZ2D/CCSD(T)	2.413	120								
	TZ2D2G2F+/MP2-AE[a]	2.381	120	344.7	0.0	38.4	31.5	370.4	98.5	79.9	4.4

[a] All electrons are correlated in MP2 calculations.

functions and an extra "f" function on lanthanum ($\alpha_g = 0.4$, $\alpha_g = 0.2$, $\alpha_f = 0.1$) and lutetium ($\alpha_g = 0.5$, $\alpha_g = 0.2$, $\alpha_f = 0.2$) atoms. Furthermore, an "sp" diffuse and an "f" polarization functions were added to halogens. For lanthanides Gaussian exponents were optimized by performing sets of RHF single-point energy calculations, while for halogens, the standard exponents were used ($F\alpha_{sp} = 0.1076$, $F\alpha_f = 1.85$ and $Cl\alpha_{sp} = 0.0483$, $Cl\alpha_f = 0.7$). This basis set is indicated as TZ2D2G2F+.

Electronic correlation effects were evaluated by adopting the computational performing MP2 treatment, while high-order effects were accounted for through the coupled-cluster single and double excitation corrected for the triples contribution by a perturbative fourth-order calculation CCSD(T). In both MP2 and CCSD(T) wave function expansions, all valence electrons, including the semicore lanthanide 5s and 5p, were correlated.

Geometries and harmonic vibrational frequencies were obtained using standard analytic or numerical gradient techniques.

Besides the scalar-relativistic effects, it is well-known that spin−orbit coupling in lanthanides is a very important issue and, for example, is much greater than ligand field effect in perturbing electronic levels of partially filled 4f shells. Therefore, it is interesting to learn how it influences the potential energy surfaces of LnX_3. Nevertheless, the presently analyzed molecules have a closed-shell electronic structure with symmetric occupation of the 4f shell (empty and filled for La^{3+} and Lu^{3+} ions, respectively). For the $^1A_1'$ molecular ground state, first-order spin−orbit effects vanish, and very small corrections for both geometry and vibrational frequencies are expected (see Appendix for a detailed analysis of spin−orbit coupling on the $LuCl_3$ molecule).

All the calculations were performed using the GAMESS code,[34] while CCSD(T) calculations were carried out using the G98 program.[35]

Nuclear Structure Calculations. Anharmonic fundamentals ($n \rightarrow n + 1$, $n = 0$) and hot transitions ($n \rightarrow n + 1$, $n \geq 1$) were computed through the correlation-corrected self-consistent-field method (PT2-VSCF) adopting a full vibrational Hamiltonian.[36]

The presently investigated molecules were characterized by a very shallow potential along the out-of-plane bending and hence, very small vibrational energy separations. Because gas-phase experiments require high temperature, levels with high quantum numbers are significantly populated. Therefore, it is useful to explore excited states with high vibrational quantum numbers ($n > 5$). The evaluation of high-lying energy levels in the PT2-VSCF approach requires simultaneous excitations of all modes; therefore, intractable grid points needed to be computed.

The LaF_3 molecule has a double-minimum potential well along the out-of-plane deformation with consequent splitting of vibrational levels. The PT2-VSCF method is not suited to deal with such situations, and the tunneling phenomenon is mistreated.

Both limitations can be overcome by adopting an effective one-dimensional Hamiltonian (EODH) to describe large-amplitude out-of-plane motion.[37,38] In this method the nuclear motions were analyzed in the framework of the so-called distinguished coordinate approach whereby the inversion path is obtained through an optimization of all the other geometrical parameters (the distance R_{Ln-X} in this case) for selected values of a single coordinate (presently, the bond angle X−Ln−X, Θ) chosen as the one more representative for such large-amplitude motion. Analogously, the symmetric stretching motion was analyzed in the framework of the one-dimensional Hamiltonian. In this case, the R_{Ln-X} interatomic distance was chosen as representative coordinate for the symmetric stretching motion.

The one-dimensional variational problem can be solved by numerical integration for any vibrational number and nth eigenstates corresponding to the energy eigenvalues, ϵ_n, are obtained. By assuming a Boltzmann population of the eigenstates and anharmonic vibrational frequencies derived from ODEH method the thermal average angle $\langle\Theta\rangle_T$ and thermal average bond length $\langle R\rangle_T$ along the out-of-plane motion and the thermal average bond length $\langle R'\rangle_T$ along the symmetric stretching are computed as a function of the temperature.

Results and Discussion

Gas-Phase Equilibrium Geometry and Electronic Structure. Optimized geometrical structures of LnX_3 molecules are listed in Table 1. For LaF_3 at the correlated level the pyramidal geometry (Figure 1) is energetically favored (~0.1 kcal/mol) with respect to the planar arrangement. For LuF_3 the C_{3v} structure is preferred at the TZ2D/MP2 level ($\Delta E = 0.001$ kcal/mol) while on improving the basis set (TZ2D2G2F+/MP2) or the wave function (TZ2D/CCSD(T)) the equilibrium geometry has D_{3h} symmetry. At all levels of theory $LaCl_3$ and $LuCl_3$ molecules assume a D_{3h} symmetry structure, but the potential

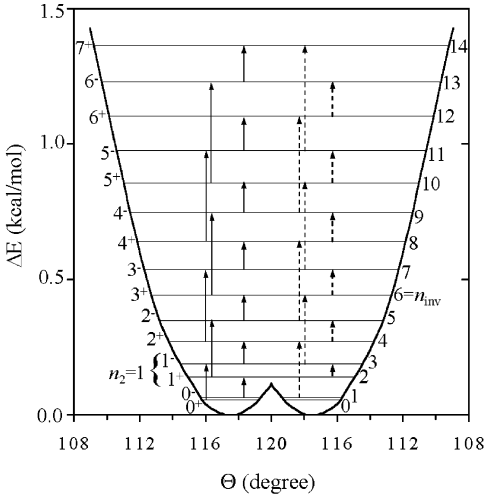

Figure 1. MP2 potential energy and lower vibrational levels for inversion of the LaF_3 molecule. The curve has been obtained through geometry optimization of the R_{La-F} distance for selected values of the bond angle Θ. The vibrational quantum number n_{inv} labels the eigenstates of the Schrödinger equation for the double well potential.

energy along the out-of-plane motion is remarkably flat especially for the $LaCl_3$ one. These data together with harmonic out-of-plane bending ν_2 frequency clearly suggest that all complexes are characterized by an extreme fluxionality and that there is a greater tendency toward planar geometries for chlorides than fluorides and on increasing lanthanide atomic number (see also structural data on GdX_3 in refs 28 and 29).

It is commonly stated that Ln−X bond is predominately ionic in character, however, there is evidence of significant covalent contribution.[17] In fact, the greater tendency toward planar geometries observed in the case of chlorides has been explained on the basis of a greater capability of the Cl^- ion (than F^-) to form π-bond.[17] The greater tendency toward planar geometries on increasing lanthanide atomic number is a direct consequence of the lanthanide contraction, i.e. the incomplete shielding of the nucleus by 4f electrons; thus, a larger effective core charge contracts and stabilizes the 5p, 5d, 6s orbitals.[39] This has two important effects: the reduction of metal ionic radius and the growth of reduction potential of Ln^{3+} ions ($Ln^{3+} + e^- \rightarrow Ln^{2+}$).[30] The former effect induces a shortening of the Ln−X bond distance on increasing the lanthanide atomic number and thus enhancing the mutual repulsion of the halogens which, in turn, opposes to the geometry bending. The latter effect gives rise to greater covalent π-interactions involving the d_{xz} and d_{yz} and the np_z halogen orbitals and hence a lower flexibility of Lu−X bonds with respect to La−X bonds toward out-of-plane distortion. In fact, the electron density contour plots of π_{La-Cl} and π_{Lu-Cl} bonds for $LaCl_3$ and $LuCl_3$ molecules (Figure 2) show greater contributions in bond formation of d_{xz} and d_{yz} metal atomic orbitals and a larger Cl_{3pz} electron density polarization toward the metal.

The present structural results are similar to ab initio data reported by Joubert et al.[24] adopting the Stuttgart RECP (4f orbitals are treated as core orbitals) and MP2 in treating electronic correlation effects. They predicted a planar structure for the entire lanthanide series of chlorides and for fluorides a slightly pyramidal geometry for LnF_3 (Ln = La−Tb), while planar structures were found for LnF_3 (Ln = Dy−Lu). Previous theoretical studies (CISD calculations reported by us on LaX_3 using LAN-RECP for lanthanum,[17] CISD calculations by Solomonik et al.[25] on LnX_3 with Cundari−Stevens RECP, and CCSD(T) calculations by Jansik et al.[27] on LaX_3 adopting Cao−

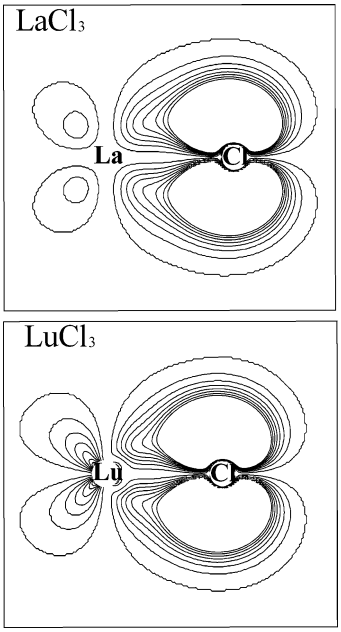

Figure 2. Electron density contour plot of π_{La-Cl} and π_{Lu-Cl} MOs in the plane containing the three-fold axes and a Ln−Cl bond. The first contour is 0.0024 e/bohr^3, and the interval between successive contours is 0.0003 e/bohr^3.

Dolg RECP and relativistic all-electron approach) led to the same conclusions on geometrical structures. Overall data indicate that ab initio results are stable versus the computational model, i.e. RECP, basis sets and electronic correlation treatment, and the present conclusions are fairly well supported. Therefore, LaF_3 and $LuCl_3$ molecules can be definitively assigned to have pyramidal and planar equilibrium structures, respectively. Both $LaCl_3$ and LuF_3 adopt planar D_{3h} symmetry structure with a very shallow minimum, but we cannot exclude a very slight deviation from planarity on increasing the theoretical level. Nevertheless, even in this unlikely case, the energy gain upon bending should be very small (<0.01 kcal/mol) and lower than the zero-point energy, and it is reasonable to think that atoms move on a D_{3h} symmetry potential well.

A large series of data based on the DFT methodologies adopting both Stuttgart and Cundari−Stevens RECP for lanthanides have been reported by Adamo et al.[21,22] and Joubert et al.[23] for LnX_3. These calculations suggest more pyramidal structures for both fluorides and chlorides with spreading of the bond angles in the range 110.8−118.9° for LnF_3 and 114.1−120.0° for $LnCl_3$, depending on the exchange and correlation potentials adopted. Nevertheless, in agreement with the present results, these data show a greater tendency toward planar geometries on going from fluorides to chlorides and on increasing the lanthanide atomic number.

The level of theory appears also important in the bond distance estimate and a general shortening is observed on passing from TZ2D/HF to TZ2D/MP2 and to TZ2D2G2F+/MP2-AE. The reduction amount depends on the specific molecule; however, it is more pronounced for chlorides than for fluorides. Conversely, R_{Ln-X} bond length slightly increased on improving electronic wave functions (TZ2D/MP2 vs TZ2D/CCSD(T)).

Gas-Phase Vibrational Frequencies. Harmonic vibrational frequencies and related IR intensities (proportional to the first derivatives of the dipole moment with respect to normal modes) at various computational levels for LnX_3 molecules are listed in Table 1. It is evident that frequencies of symmetric stretching ν_1, double degenerate asymmetric stretching ν_3, and scissors-

TABLE 2: Anharmonic PT2-VSCF Vibrational Transitions Calculated at the RHF and MP2 (in parentheses) Levels for the LaF_3 and LuF_3 in the Gas Phase

	ν_1/cm^{-1}		ν_2/cm^{-1}		ν_3/cm^{-1}		ν_4/cm^{-1}	
transition	ω	$\Delta\omega^a$	ω	$\Delta\omega$	ω	$\Delta\omega$	ω	$\Delta\omega$
				LaF_3				
harmonic	523.4		10.0		514.8		125.9	
	(524.3)		(44.9)		(516.3)		(120.9)	
0 → 1	520.3		24.7		510.3		125.3	
	(520.2)		(38.9)		(511.7)		(120.4)	
1 → 2	519.8	−0.5	33.4	8.7	508.3	−2.0	125.1	−0.2
	(519.3)	(−0.9)	(41.1)	(2.2)	(509.6)	(−2.1)	(120.2)	(−0.2)
2 → 3	519.4	−0.5	38.1	4.7	506.2	−2.1	124.8	−0.3
	(518.8)	(−0.5)	(44.5)	(3.4)	(507.4)	(−2.2)	(120.1)	(−0.1)
3 → 4	519.6	0.2	41.5	3.4	504.4	−1.8	124.7	−0.1
				LuF_3				
harmonic	596.0		58.6		584.3		145.8	
	(594.8)		(20.1)		(585.2)		(149.6)	
0 → 1	592.1		60.5		579.2		145.4	
	(590.0)		(30.3)		(579.1)		(148.0)	
1 → 2	591.4	−0.7	62.4	1.9	576.9	−2.3	145.2	−0.2
	(589.5)	(−0.5)	(37.0)	(6.7)	(576.6)	(−2.5)	(148.3)	(0.3)
2 → 3	590.9	−0.5	64.6	2.2	574.6	−2.3	145.1	−0.1
	(589.4)	(−0.1)	(47.7)	(10.7)	(573.7)	(−2.9)	(148.1)	(−0.2)
3 → 4	590.6	−0.3	66.7	2.1	572.2	−2.4	145.1	0.0
4 → 5	590.6	0.0	68.5	1.8	569.8	−2.4	145.1	0.0
5 → 6	590.8	0.2	70.4	1.9	567.4	−2.4	145.2	0.1

[a] $\Delta\omega = \omega_{n+1} - \omega_n$ (n = vibrational quantum number).

type bending ν_4 slightly depend on the computational level (the maximum difference observed is 9.9 and 17.0 cm^{-1} for fluorides and chlorides, respectively). Conversely, the ν_2 out-of-plane bending changes significantly on passing from TZ2D/HF to TZ2D/MP2 wave functions, indicating a substantial potential energy modification. The close TZ2D/MP2 and TZ2D2G2F+/MP2-AE harmonic frequencies justify the usage of the TZ2D/MP2 theory level for the subsequent nuclear structure analysis.

Potential energy curves along the ν_1, ν_3, and ν_4 normal modes are more or less parabolic. Anharmonic corrections are generally small, and the adoptions of ODEH or PT2-VSCF methods allow a fine refinement. Conversely, the potential energy curves along the out-of-plane ν_2 mode for all molecules have a rather flat and anharmonic form (Figure 1 for LaF_3), and the adoption of more rigorous PT2-VSCF and ODEH treatments is mandatory.

For all molecules hereby considered, on passing from harmonic to fundamental frequencies and hot transitions (Tables 2 and 3), it can be seen that anharmonicities are actually small for ν_1, ν_3, and ν_4 normal modes. The data slightly depend on electronic wave functions (HF or MP2), and some general trends can be drawn. The vibrational frequencies of in-plane bending (ν_4) are almost invariant upon inclusion of anharmonic terms, thus indicating an almost pure harmonic potential. The frequency of stretching modes (ν_1 and ν_3) drop on passing from harmonic to fundamentals and to hot transitions, indicating a small positive anharmonicity constant. Furthermore, anharmonicities are more pronounced for the asymmetric stretching. Unexpectedly, vibrational levels of the ν_1 mode and to a lesser extent those of the ν_3 mode computed at the HF level do not crowd together more closely for the highest vibrational quantum numbers. This is an artifact of HF in the evaluation of potential energy grids used in subsequent PT2-VSCF calculations. However, this effect is absent or less pronounced when correlation effects are included.[29]

The out-of-plane bending frequency shows remarkable negative anharmonicities even for the lowest vibrational levels because of the strongly anharmonic potential energy associated (Figure 1). In this context the potential energy curve can be classified in three discernibly different shapes. In the simplest

TABLE 3: Anharmonic PT2-VSCF Vibrational Transitions Calculated at the $LaCl_3$ and $LuCl_3$ in the Gas Phase

	ν_1/cm^{-1}		ν_2/cm^{-1}		ν_3/cm^{-1}		ν_4/cm^{-1}	
transition	ω	$\Delta\omega^a$	ω	$\Delta\omega$	ω	$\Delta\omega$	ω	$\Delta\omega$
				$LaCl_3$				
harmonic	305.9		31.8		325.1		71.7	
	(311.8)		(1.9)		(337.0)		(68.8)	
0 → 1	304.7		32.5		323.1		71.7	
	(310.6)		(13.4)		(334.9)		(68.9)	
1 → 2	304.3	−0.4	33.2	0.7	322.2	−0.9	71.6	−0.1
	(310.2)	(−0.4)	(20.1)	(6.7)	(333.7)	(−1.2)	(68.7)	(−0.2)
2 → 3	304.0	−0.3	34.1	0.9	321.4	−0.8	71.6	0.0
3 → 4	303.7	−0.3	35.0	0.9	320.6	−0.8	71.6	0.0
4 → 5	303.4	−0.3	35.8	0.8	320.0	−0.6	71.7	0.1
5 → 6	303.2	−0.2	36.8	1.0	319.5	−0.5	71.7	0.0
6 → 7	303.1	−0.1	37.2	0.4	319.1	−0.4	71.8	0.1
7 → 8	303.3	0.2	38.2	1.0	318.9	−0.2	72.1	0.3
				$LuCl_3$				
harmonic	335.8		54.0		353.4		82.9	
	(341.6)		(42.1)		(364.4)		(80.7)	
0 → 1	334.3		54.1		351.2		83.1	
	(340.4)		(42.2)		(362.4)		(80.8)	
1 → 2	333.9	−0.5	54.3	0.2	350.3	−0.9	83.2	0.1
	(340.0)	(−0.4)	(42.6)	(0.4)	(361.5)	(−0.9)	(80.9)	(0.1)
2 → 3	333.4	−0.4	54.5	0.2	349.5	−0.8	83.3	0.1
	(339.5)	(−0.5)	(43.1)	(0.5)	(360.7)	(−0.8)	(81.0)	(0.1)
3 → 4	333.0	−0.4	54.8	0.3	348.7	−0.8	83.4	0.1
	(339.1)	(−0.4)	(43.6)	(0.5)	(359.8)	(−0.9)	(81.2)	(0.2)
4 → 5	332.7	−0.3	55.1	0.3	348.0	−0.7	83.6	0.2
	(338.4)	(−0.7)	(44.1)	(0.5)	(358.8)	(−1.0)	(81.3)	(0.1)
5 → 6	332.5	−0.2	55.4	0.3	347.5	−0.5	83.8	0.2
6 → 7	332.4	−0.1	55.7	0.3	347.3	−0.2	84.1	0.3
7 → 8	332.6	0.2	56.1	0.4	347.3	0.0	84.3	0.2

[a] $\Delta\omega = \omega_{n+1} - \omega_n$ (n = vibrational quantum number).

case, molecules adopt D_{3h} symmetry with "steep" wall potential ($LaCl_3$/HF, LuF_3/HF, $LuCl_3$/HF, and $LuCl_3$/MP2); thus, there is a moderate increase of ν_2 frequency on going from harmonic to fundamental and to hot transitions. The PT2-VSCF method allows estimation of vibrational levels with high quantum numbers ($n \leq 8$). In the second case, molecules adopt D_{3h} symmetry with a very shallow well (LaF_3/HF and $LaCl_3$/MP2) or C_{3v} symmetry with vanishing potential barrier (LuF_3/MP2). These molecules are characterized by huge differences between harmonic, fundamental, and hot transitions. In such situations the PT2-VSCF method requires dense grids to get reasonable accuracy, and in any case, only the lowest vibrational levels ($n \leq 4$) can be obtained. The adoption of the EODH to describe out-of-plane motion of a "nonrigid molecule" is more fruitful. The LaF_3/MP2 potential energy (the third case) is characterized by a relatively high inversion barrier (~0.1 kcal/mol), therefore, the lowest two vibrational levels are below the potential maximum, while energy levels higher than $n \geq 2$ lie above (Figure 1). Also in this case computed fundamental and hot transitions show remarkable negative anharmonicity. However, it should be noted that the potential energy grid used in PT2-VSCF calculations has been derived starting from one of the two energy minima and does not adequately describe the symmetry of the potential energy well; thus, the tunneling through the barrier is not reproduced by the PT2-VSCF method. Also in this case the adoption of the EODH method produces more appropriate results.

EODH vibrational levels for the ν_2 out-of-plane motion of all presently analyzed molecules (Table 4) show a remarkable increase of energy separation between adjacent states as the vibrational quantum number increases in good agreement with PT2-VSCF data. For the extreme $LaCl_3$ case, the computed 10

TABLE 4: Selected Anharmonic ODEH Vibrational States Energy for the ν_2 Out-of-Plane Bending Mode of LnX_3 Molecules

n	LaF_3 cm^{-1}	LuF_3 cm^{-1}	$LaCl_3$ cm^{-1}	$LuCl_3$ cm^{-1}	n	LaF_3 cm^{-1}	LuF_3 cm^{-1}	$LaCl_3$ cm^{-1}	$LuCl_3$ cm^{-1}
0	20.0	8.8	4.4	21.1	21	828.2	1137.7	524.5	976.4
1	22.1	32.1	15.8	63.6	30	1346.0	1796.9	828.9	1428.7
2	49.4	64.5	30.9	106.4	31	1407.2	1874.2	864.7	1480.8
3	66.7	101.7	48.1	149.4	40	1987.7	2603.0	1203.6	1970.1
4	92.7	142.7	67.0	192.7	41	2055.3	2687.6	1243.2	2026.9
10	300.9	442.5	204.7	459.0	50	2691.7	3483.9	1618.0	2557.9
11	342.4	499.2	230.7	504.5	51	2765.7	3576.4	1661.9	2618.2
20	774.8	1068.9	492.7	927.9					

$\rightarrow$ 11 (26.0 cm^{-1}), 30 $\rightarrow$ 31 (35.8 cm^{-1}), and 50 $\rightarrow$ 51 (43.9 cm^{-1}) hot transitions are respectively 2, 3, and 4 times greater than the fundamental 0 $\rightarrow$ 1 (11.4 cm^{-1}).

For D_{3h} symmetry molecules, transitions between adjacent levels of the ν_2 normal mode are IR allowed by both the symmetry rule (there is an alternation of the A_2'' and the A_1' symmetry states) and the $\Delta n = \pm 1$ selection rule. Even though LuF_3 possesses a double-minimum potential at the TZ2D/MP2 level, the $n = 0$ eigenstate of the ν_2 mode is above the inversion barrier; therefore, it can be treated as a single-minimum system, and the above-mentioned IR selection rules remain valid. For the LaF_3 molecule the inversion energy barrier height is sufficient to observe the phenomenon of quantum mechanical tunneling.[40,41] The barrier penetration induces a great interaction between the identical sets of vibrational levels into two limbs of the potential curve. This interaction splits the n_2 levels of the "rigid nonplanar molecule" into two components, n_2^+ and n_2^-. In Figure 1 the ODEH inversion states are numbered both by the n_2 value for the "rigid nonplanar molecule" level, with which they correlate, and by the quantum number n_{inv}. The use of the quantum number n_{inv} (which gives the total number of nodes in the inversion wave function) allows us to treat LaF_3 as a planar molecule with a highly anharmonic out-of-plane vibration. By using this quantum number the vibrational and rotational selection rules for allowed optical transitions are easily formulated.[41]

The molecular symmetry group of inverting LaF_3 molecule is D_{3h}(M). The symmetry of the vibrational eigenfunctions are A_1' (the total symmetric) for levels with n_{inv} even, while states with n_{inv} odd have the symmetry A_2''. The vibrational-inversion spectrum must satisfy the symmetry selection rule Δn_{inv} = odd. The $\Delta n_{inv} = (n_{inv} \rightarrow n_{inv} + 3) = \pm 3$ with n_{inv} even and $\Delta n_{inv} = (n_{inv} \rightarrow n_{inv} + 1) = \pm 1$ with n_{inv} odd conditions should give rise to two band envelopes separated in the IR spectrum. These transitions, correlated with the $\Delta n_2 = (n_2 \rightarrow n_2 + 1)$ bands of the rigid nonplanar molecule, should have a high transition probability (they are indicated by solid arrows in Figure 1). The $\Delta n_{inv} = (n_{inv} \rightarrow n_{inv} + 3) = \pm 3$ with n_{inv} odd and $\Delta n_{inv} = (n_{inv} \rightarrow n_{inv} + 1) = \pm 1$ with n_{inv} even conditions should also give rise two bands overlapping with those previously discussed. However these bands, correlated with the $\Delta n_2 = (n_2 \rightarrow n_2 + 2) = \pm 2$ and $\Delta n_2 = (n_2 \rightarrow n_2) = 0$ transitions of the rigid nonplanar molecule, should have a low transition probability (they are indicated by dashed arrows in Figure 1). These predictions are very important since they could provide an additional simple tool to distinguish between planar (single-band envelope) and pyramidal structure (double-band envelope) of molecules in the gas-phase.

A similar energy level separation for the out-of-plane bending of the LaF_3 molecule has been reported by Solomonik et al.;[25] however, no analysis about allowed optical transitions has been done. The inversion doubling of the out-of-plane bending is a well-documented common feature of nonplanar tricoordinate molecules in the electronic ground state (NH_3, PH_3, SiH_3, and amines)[40,42,43] or in excited states (OCF_2, $SCCl_2$, SCF_2, OCFH, etc).[44−46] However, to our knowledge, this phenomenon has never been observed for metal trihalides.

Comparison of Theoretical and Gas-Phase Experimental Frequencies. The high temperature (1350 K) gas-phase IR spectrum of $LaCl_3$ shows two broad bands: the first in the 280−340 cm^{-1} range exhibiting a flattened band shape on the low-frequency wing and the second in the 30−75 cm^{-1} range.[6,8] For trigonal planar D_{3h} structure only the ν_2, ν_3, and ν_4 modes are IR active with the intensity ratio 1.0:3.0:0.2, respectively, while the ν_1 is inactive (Table 1). Therefore, the band located approximately at 320 cm^{-1} is assigned to the ν_3 normal mode, while the band envelope in the range 30−75 cm^{-1} contains absorptions of both ν_2 and ν_4 modes. For the $LaCl_3$ symmetric top molecule, the ν_3 is a perpendicular vibration ($\Delta n_3 = \pm 1$; $\Delta J = 0, \pm 1$; $\Delta K = \pm 1$) and gives rise to many sets of *P*, *Q*, and *R* unresolvable branch lines which produce a consistent peak broadening. However, this is not the only reason for the presence of such a large absorption. In fact, the anharmonicity shifts the hot bands (Table 3) by ~1 cm^{-1}, thus producing a significant absorption enlargement. In addition, because high levels are less populated (for the ν_3 mode, Boltzmann population at 1350 K of nine lowest states relative to the fundamental one are: 1.00, 0.71, 0.50, 0.36, 0.25, 0.18, 0.13, 0.09, and 0.07), the associated hot band intensities decrease, thus rendering the peak asymmetric, in agreement with the absorption band shape in the experimental IR spectrum.

The ν_2 is a parallel vibration ($\Delta n_2 = \pm 1$; $\Delta J = 0, \pm 1$; $\Delta K = 0$), and each transition gives rise to a single set of *P*, *Q*, and *R* branches. However, as discussed above, this mode suffers from a strong negative anharmonicity, and levels over $n = 50$ are significantly occupied, thus giving rise to tens of *PQR* structures separated by the anharmonic hot band shift (Tables 3 and 4). This allows us to explain the large band (starting from ~30 up to ~75 cm^{-1}) observed in gas-phase IR spectrum. The ν_4 falls in the same region of the ν_2 absorption; it is a perpendicular vibration and gives rise to complicated *PQR* branch lines. The ν_4 mode is much less intense than ν_2 and is only slightly anharmonic; therefore, it should give a "sharp" signal centered at ~70 cm^{-1} superimposed on the main ν_2 band. In fact, the large band in the 30−75 cm^{-1} associated with the ν_2 mode shows a shoulder at ~70 cm^{-1} which can be ascribed to the ν_4 absorption.

Unfortunately, gas-phase IR spectra of LaF_3, LuF_3, and $LuCl_3$ have not been reported until now; therefore, a detailed comparison of experimental and theoretical analysis is hampered. Nevertheless, some predictions can be made on the basis of present theoretical data.

For $LuCl_3$, a broad and asymmetric band centered at ~350 cm^{-1} is expected since a similar shift is computed for the ν_3 anharmonic frequencies of $LuCl_3$ and $LaCl_3$. The ν_2 band envelope in the IR spectrum should appear at wavenumbers higher than those observed for $LaCl_3$. Furthermore, because of the lower anharmonicity frequency shift and less population of high-excited levels, the ν_2 absorption in the $LuCl_3$ spectrum should be less broad. The ν_4 band should appear as a shoulder on the high-frequency wing of the ν_2 band at ~81 cm^{-1}.

The more intense band in the IR spectra of LaF_3 and LuF_3 would be the ν_3 (~515 and ~585 cm^{-1}, respectively). Despite the more consistent anharmonic frequency shift (compared to $LnCl_3$), the bandwidth should be similar to those observed for lanthanide chlorides (~50 cm^{-1}) because the higher vibrational

TABLE 5: Calculated Average Bond Lengths and Bond Angles of LnX_3 over the Out-of-Plane and the Symmetric Stretching Vibrations at the Experimental ED Temperature; Experimental Average Structural Parameters (R_g and Θ_{vg}) and Equilibrium Geometrical Data (in parentheses) Are Reported for Comparison

		computation			experiment[a]	
		$\langle R\rangle_T$[b]/Å	$\langle\Theta\rangle_T$[b]/deg	$\langle R'\rangle_T$[c]/Å	R_g/Å	Θ_{vg}/deg
LaF_3	TZ2D/MP2	(2.168)	(117.6)			
	1500 K	2.165	114.9	2.173	2.22(3)	120
LuF_3	TZ2D/MP2	(1.966)	(119.7)			
	1500 K	1.961	116.0	1.971		
$LaCl_3$	TZ2D/MP2	(2.623)	(120)			(120)[d]
	1100 K	2.616	115.6	2.628	2.589(6)	116.7(1.2)
$LuCl_3$	TZ2D/MP2	(2.397)	(120)			(120)[d]
	1070 K	2.393	117.3	2.400	2.403(5)	117.9(1.3)

[a] Experimental data are taken from refs 2, 3, and 50. [b] Thermal average structure over the out-of-plane bending. [c] Thermal average distance over the symmetric stretching. [d] Equilibrium bond angle estimated from ED data.[2,3]

step prevents a significant population of vibrational levels higher than $n = 4$. The ν_1 signal should be absent (LuF_3) or very weak (LaF_3) and hidden by the very strong ν_3 band. Also for LnF_3 molecules, the ν_2 mode should raise the lowest frequency absorption. It should be very broad because of the huge anharmonicity. For LuF_3 the ν_2 mode should yield to a rather "sharp" single-band envelope ($\sim$40 cm^{-1}), while LaF_3 should give rise to a large double-band envelope overlapping in some degree because of the tunneling effect discussed above. For the LuF_3 molecule the $\nu_2-\nu_4$ frequency separation is more conspicuous than that observed for $LnCl_3$ ($\sim$60 vs $\sim$30 cm^{-1}), and presumably the ν_4 absorption would appear as separated single weak band.

Comparison of Theoretical and Gas-Phase Experimental Geometrical Data. The comparison of theoretical and experimental geometrical parameters is not straightforward. In fact, the equilibrium structure generally derived in computational studies corresponds to the minimum of the Born−Oppenheimer potential energy surface, while in ED studies the thermal average bond lengths R_{Ln-X} (R_g) and R_{X-X} are directly measured, and the "virtual" thermal average bond angle (Θ_{vg}) is indirectly derived.[1] Two ways are possible to make a reasonable theoretical/experimental comparison: (i) the experimental ED data should be handled to derive both equilibrium bond length and bond angle,[1,5] and (ii) vibrational effects should be included in the calculations to get average structure.[47,48]

Recently, a planar equilibrium structure D_{3h} has been derived for $LaCl_3$ and $LuCl_3$ from ED data analysis through a semiempirical dynamic model, which takes into account the ν_2 anharmonicities.[2,3] This estimation is in full agreement with the present theoretical results on the $LaCl_3$ and $LuCl_3$ molecules. No experimental data have been reported on the R_e(Ln−Cl) and on the symmetry of the equilibrium structure of fluorides. Therefore, the ab initio theoretical derivation of thermal average structures becomes a very important issue.

For all molecules presently considered, the thermal average bond angle $\langle\Theta\rangle_T$ computed along the out-of-plane motion at experimental ED temperature is lower than the equilibrium Θ_e's, thus giving rise to C_{3v} structures in all cases (Table 5). Our estimate of thermal average structures is in good agreement with gas-phase ED data on lanthanide trichlorides that suggest pyramidal structures for all cases. Also, numerical comparison of thermal average angle Θ_{vg} is good (Table 5); thus, theoretical data for $LaCl_3$ and $LuCl_3$ (115.6° and 117.3°, respectively) well reproduce experimental gas-phase ED results (116.7(1.2)° and 117.9(1.3)°, respectively).

Electron diffraction studies on LnF_3 are scarce because of technical problems implicit in the high temperature required for sublimation (>1500 K). Consequently, a detailed comparison of theoretical and experimental structure is hampered (the past ED measurements reported in 1959 suggested a planar structure for LaF_3).[49]

As the molecule moves away from the equilibrium angle (Θ decrease), there is a gradual reduction of the optimal R_{Ln-X} distance, and for $\Theta = 100°$ the R_{Ln-X} decreases by $\sim$0.025 Å for both fluorides and chlorides. Therefore, when the Ln−X bond length is averaged along the ν_2 mode, there is a significant reduction ($\sim$0.005 Å) with respect to the equilibrium structure (Table 5).

Even though anharmonicities on stretching modes are small, they directly affect R_g parameters and of course cannot be ignored for the correct description of the vibrational average structure. The ν_1 and ν_3 normal modes show small "positive" anharmonic forms; thus, when the bond distance is averaged along these modes, it should increase with respect to the equilibrium value. The one-dimensional nature of the ν_1 normal mode allows a practicable computational analysis of its effect on thermal average distance. For all cases, the population of high excited vibrational states (up to $n = 4$ for fluorides and up to $n = 7$ for chlorides) results in MP2 thermal average distances $\langle R'\rangle_T$ slightly larger ($\sim$0.005 Å) than R_e at the temperature of ED experiments. The double degenerate asymmetric stretching, ν_3, is more anharmonic than the symmetric stretching (Tables 2 and 3); therefore, a substantial bond lengthening (at least 0.01 Å or even higher) should occur when the structure is averaged over this mode.

Assuming a simple additive effect due to the thermal vibrational modulation discussed above, the bond length shortening due to the out-of-plane bending ($\sim$0.005 Å) would be compensated by the lengthening due to the symmetric stretching ($\sim$0.005 Å), while the asymmetric stretching should infer a lengthening of $\sim$0.01 Å. In summary, we may conclude that the bond distance averaged over all vibrations should be greater than the equilibrium bond distance by $\sim$0.01 Å. An addition of 0.01 Å to our best (TZ2D2G2F+/MP2-AE) estimated R_e of both $LaCl_3$ and $LuCl_3$ leads to a theoretical thermal average distance close to that measured by ED (2.613 Å vs 2.589(6) Å and 2.391 Å vs 2.403(3) Å for $LaCl_3$ and $LuCl_3$, respectively).[2,3]

Geometry of Molecules Trapped in Inert-Gas Matrices. IR and Raman measurements of isolated reactive molecules in inert matrices at cryogenic temperatures doubtless are important tools for the structural characterization of LnX_3 species,[9−13] since the quenched rotational motion gives IR/Raman spectra that are greatly simplified compared to those obtained in gas-phase at high temperatures. Nevertheless, the spectra analysis is not straightforward because of additional experimental problems that sometimes might lead to controversial interpretation.[10−13] In this perspective, the following various aspects should be considered. (i) Host−guest interactions in matrices are generally substantial; thus, there is an ample shift of band frequencies on changing inert-gas, especially for large amplitude modes. (ii) Isolated molecules can occupy different matrix sites; thus, the molecular orientation and shape might depend on the disposition of neighbor matrix units, and sometime various absorptions can be associated to a normal mode. (iii) For strongly interacting matrices such as N_2, there is also evidence of the ν_3 degeneracy removal due to lowering of the molecular symmetry. (iv) Depending on the experimental conditions in matrix/molecules preparation, oligomerization can significantly occur, giving rise to additional absorptions.

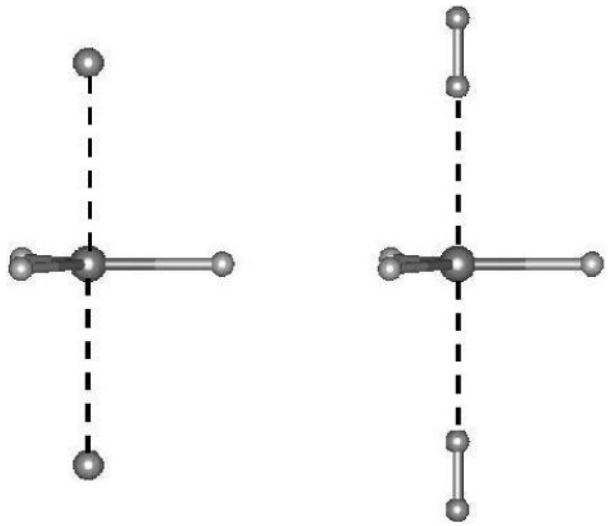

Figure 3. Schematic view of molecular structures of $LnX_3 \cdot Ne_2$ and $LnX_3 \cdot (N_2)_2$ complexes.

From a computational point of view the simulation of host−guest interactions is a challenging task, and various treatments have been proposed.[50,51] In a simplified view two effects should be considered, (i) a local static interaction between the molecules and the neighbor matrix units which might lead to the formation of a "complex" and (ii) a nonlocal dynamic effect due to the coupling of extended solid vibrations and intramolecular modes.

In a previous study on GdX_3 systems we modeled the local static matrix effects through a simple coordination of one ($GdX_3 \cdot IG$) and two ($GdX_3 \cdot IG_2$) inert-gas atoms (or molecules).[28,29] These data show that the coordination energy of two inert-gas atoms (Ne, Ar, and Xe) or molecules (N_2) is almost double than that obtained for the coordination of a single species. Therefore, the high Lewis acidity of GdX_3 is not quenched by the coordination of a single inert-gas unit, and the complexation of two species is the process energetically favored.[28,29] Presently, we restricted our analysis only to the coordination of two inert-gas units since $LnX_3 \cdot IG_2$ complexes better simulate host−guest interactions in real systems. This model, initially proposed by Schleyer et al.[50] for $CaH_2 \cdot L$ and $CaF_2 \cdot L$ systems, despite its simplicity, allows a rationalization of important experimental spectroscopic features.

Figure 3 shows schematic representations of $LnX_3 \cdot IG_2$ (IG = Ne, Ar, Xe, and N_2) structures, whereas Table 6 collects metrical parameters and complex formation energies ($LnX_3 + 2IG \rightarrow LnX_3 \cdot IG_2 + \Delta E$) obtained at RHF and MP2 levels. Furthermore, Figure 4 displays MP2 complex formation energies (corrected for basis set superposition error) as a function of the lanthanide atom, including results previously reported for $GdX_3 \cdot IG_2$ complexes.[28,29]

The complexation energies computed at MP2 level are considerably greater than the HF ones, thus confirming the crucial role of electron correlation in describing weak van der Waals interactions (ion-induced-dipole) between molecules and host-matrix. Energetic data indicate that inert-gas atoms (or molecules) strongly coordinate the metal and the binding energy depends on inert-gas species, lanthanide atoms, and bonded halides. Some general features can be derived from analysis of data reported in Table 6 and Figure 4.

There is a gradual growth of stabilization energy on passing from $LnX_3 \cdot Ne_2$ to $LnX_3 \cdot Ar_2$ and $LnX_3 \cdot Xe_2$ complexes, while a more pronounced increase is found for the $LnX_3 \cdot (N_2)_2$ systems. This behavior reflects the enhanced polarizability of inert-gas units, $N_2 \gg Xe > Ar > Ne$. Computed Mulliken charges on atoms for all $LnX_3 \cdot IG_2$ complexes indicate a considerable transfer of electron density from the IG_2 framework to the LnX_3 molecule. This leads to the formation of a weak Ln- - -IG bond, and its strength qualitatively parallels the stabilization energy trend reported in Figure 4 (the bond order is ∼0.05, ∼0.13, ∼0.14, and ∼0.19 for $LnX_3 \cdot Ne_2$, $LnX_3 \cdot Ar_2$, $LnX_3 \cdot Xe_2$, and $LnX_3 \cdot (N_2)_2$, respectively).

Because of the greater electronegativity of fluorine with respect to chlorine atoms, the charge on metal is higher in LnF_3 than in $LnCl_3$; thus, we would have expected greater complexation energy for $LnF_3 \cdot IG_2$. Nevertheless, a reverse order has been found which can be ascribed to greater steric nonbonding repulsive interactions between halogen pairs and inert-gas units in $LnF_3 \cdot IG_2$ complexes.

The complex formation energy for $LnX_3 \cdot Ne_2$, $LnX_3 \cdot Ar_2$, and $LnX_3 \cdot Xe_2$ series is almost insensitive to the metal (Figure 4), thus indicating that matrix effects are very similar in a homologous series. In contrast, for $LnX_3 \cdot (N_2)_2$ complexes, there is a gradual rise of stabilization energy (ΔE becomes more exothermic) on increasing the lanthanide atomic number, thus suggesting that host−guest interactions augment across the lanthanide series and the nitrogen is not actually an inert-gas matrix.

All the $LnX_3 \cdot IG_2$ complexes have trigonal bipyramid arrangement with D_{3h} symmetry (except the $LaF_3 \cdot Ne_2$ at MP2 level, Table 6); thus, the symmetric coordination of two inert-gas molecules invariably leads to planar LnX_3 framework. These data clearly indicate that inert-gas matrices strongly affect the molecular structure of floppy molecules such as lanthanide trihalides and the geometry deduced in the gas-phase might be different from that obtained in matrices. For the $LaF_3 \cdot Ne_2$, the computed D_{3h} structure at MP2 level is unstable, and equilibrium geometry has C_{3v} symmetry with a slightly pyramidal LnX_3 framework and asymmetric coordination of Ne atoms. Present calculations for isolated molecules show that the LaF_3 has the greatest propensity toward adopting pyramidal structure. This tendency is not completely quenched by the weak coordinating Ne atoms. Although results on $LnX_3 \cdot IG_2$ complexes (with the exception of the $LaF_3 \cdot Ne_2$) suggest planar structure for LnF_3 in matrices (in contrast to data obtained for isolated species), it is premature to conclude that LnF_3 molecules in matrices assume planar structure, because of the simplicity of the adopted model. However, to date this aspect does not seem to be fully settled experimentally.[10−13]

The R_{Ln-IG} distance decreases substantially on passing from RHF to MP2 level (∼0.3 Å, Table 6), indicating an enhanced LnX_3-IG_2 interaction in agreement with the increased complexation energy discussed above. In addition, the R_{Ln-IG} separations are ubiquitously longer in fluoride than in chloride complexes, accordingly to the reduced complexation energy. This effect may be explained by considering the reduced room at the metal center. Furthermore, because of the lanthanide contraction, the R_{Ln-IG} distance diminishes for heavier lanthanides.

The coordination of inert-gas atoms (or molecules) induces a significant increase of the Ln−X bond distances. In fact, the transfer of electron density from IG_2 to LnX_3 moiety slightly destabilizes LnX_3 molecular orbitals thus weakening Ln−X bonds. The lengthening parallels the complexation energy, it increases on passing from the RHF to MP2 wave functions, and it grows along the series $LnX_3 \cdot Ne_2 < LnX_3 \cdot Ar_2 < LnX_3 \cdot Xe_2 < LnX_3 \cdot (N_2)_2$ (percentages of lengthening at MP2 level are: ∼0.2%, ∼0.4%, ∼0.5%, and ∼0.7%, respectively).

TABLE 6: Calculated Equilibrium Bond Lengths and Bond Angles for LnX_3, and $LnX_3 \cdot IG_2$ (IG = Ne, Ar, Xe, and N_2) Systems; the Stabilization Energies Have Been Computed with Respect to Isolated LaX_3 and LuX_3 Molecule and Isolated Inert-Gas Units

	RHF				MP2			
	R_{Ln-X}/Å	Θ/deg	R_{Ln-IG}/Å	ΔE^a/kcal mol^{-1}	R_{Ln-X}/Å	Θ/deg	R_{Ln-IG}/Å	ΔE^a/kcal mol^{-1}
LaF_3	2.169	120			2.169	117.6		
$LaF_3 \cdot Ne_2$	2.171	120	3.206	−1.2 (−0.7)	2.175	119.7	2.976 2.968	−3.4 (−1.6)
$LaF_3 \cdot Ar_2$	2.173	120	3.550	−1.9 (−1.4)	2.178	120	3.275	−5.6 (−3.7)
$LaF_3 \cdot Xe_2$	2.175	120	3.910	−2.4 (−2.2)	2.181	120	3.607	−8.9 (−5.4)
$LaF_3 \cdot (N_2)_2$	2.181	120	3.050	−8.9 (−7.9)	2.185	120	2.890	−15.9 (−12.1)
LuF_3	1.984	120			1.966	119.7		
$LuF_3 \cdot Ne_2$	1.986	120	2.746	−2.0 (−1.2)	1.970	120	2.568	−7.5 (−2.8)
$LuF_3 \cdot Ar_2$	1.989	120	3.165	−2.8 (−2.3)	1.974	120	2.873	−9.8 (−5.5)
$LuF_3 \cdot Xe_2$	1.991	120	3.568	−3.7 (−3.1)	1.976	120	3.258	−13.0 (−7.0)
$LuF_3 \cdot (N_2)_2$	1.996	120	2.666	−13.9 (−12.6)	1.981	120	2.505	−27.5 (−18.6)
$LaCl_3$	2.652	120			2.623	120		
$LaCl_3 \cdot Ne_2$	2.655	120	3.153	−1.4 (−0.9)	2.626	120	2.910	−4.5 (−2.3)
$LaCl_3 \cdot Ar_2$	2.659	120	3.460	−2.5 (−1.9)	2.630	120	3.193	−8.0 (−5.7)
$LaCl_3 \cdot Xe_2$	2.663	120	3.809	−3.4 (−3.2)	2.635	120	3.518	−12.9 (−8.6)
$LaCl_3 \cdot (N_2)_2$	2.668	120	2.978	−11.2 (−10.2)	2.637	120	2.820	−21.0 (−16.3)
$LuCl_3$	2.439	120			2.397	120		
$LuCl_3 \cdot Ne_2$	2.444	120	2.801	−1.5 (−0.6)	2.402	120	2.566	−7.7 (−2.0)
$LuCl_3 \cdot Ar_2$	2.447	120	3.234	−2.3 (−1.6)	2.408	120	2.867	−10.8 (−5.6)
$LuCl_3 \cdot Xe_2$	2.451	120	3.607	−3.4 (−2.6)	2.412	120	3.243	−15.6 (−8.3)
$LuCl_3 \cdot (N_2)_2$	2.461	120	2.645	−14.8 (−13.0)	2.416	120	2.465	−32.4 (−21.0)

[a] Stabilization energies corrected for basis set superposition error are given in parentheses.

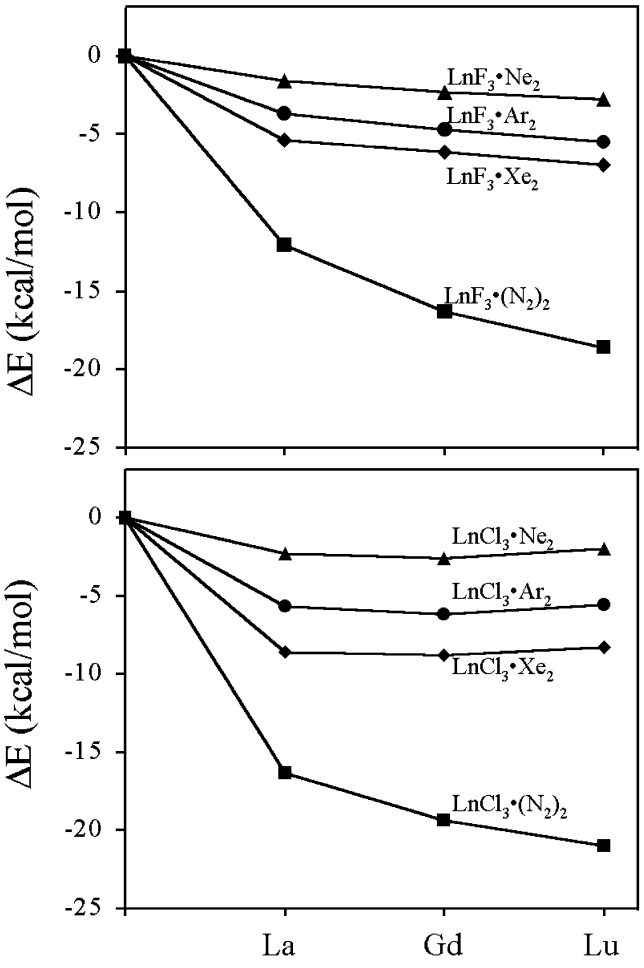

Figure 4. Calculated LnX_3-IG_2 interaction energy for $LnX_3 \cdot IG_2$ (Ln = La, Gd, Lu) complexes at MP2 level. Data for $GdX_3 \cdot IG_2$ complexes have been taken from refs 28 and 29.

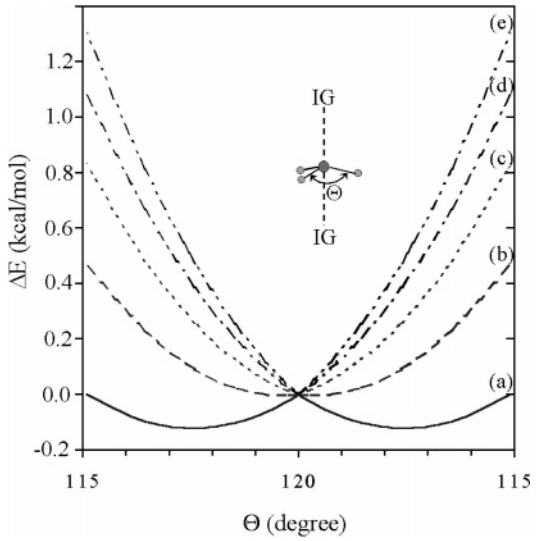

Figure 5. Potential energy curves for the isolated LaF_3 molecule, solid line (a), and $LnF_3 \cdot IG_2$ complexes broken lines (b = Ne; c = Ar; d = Xe; e = N_2) as a function of the bond angle Θ. The R_{La-F} and R_{La-IG} distances have been fixed to the optimized MP2 equilibrium structure.

Harmonic Vibrational Frequencies of Molecules Trapped in Inert-Gas Matrices. Figure 5 reports inversion potential energy curves (fixed R_{La-F} and R_{La-IG} distances) for the isolated LaF_3 species and for $LaF_3 \cdot IG_2$ complexes. The isolated LaF_3 molecule and the $LaF_3 \cdot Ne_2$ complex show a double-minimum potential well, but the energy barrier to passage of the lanthanum atom through the F_3 plane is considerably reduced for the latter system (0.12 vs 0.003 kcal/mol). In contrast the $LaF_3 \cdot Ar_2$, $LaF_3 \cdot Xe_2$, and $LaF_3 \cdot (N_2)_2$ complexes show single-minimum energy curves with the steepest wall for the third one. Therefore, weak interactions of LnX_3 molecules with the inert-gas matrices profoundly affect the out-of-plane bending, and molecules become stiffer upon increasing the $LnX_3 \cdot\cdot IG_2$ interaction energy (Table 7). For the LaF_3/MP2 case, there is a substantial lowering of the ν_2 harmonic frequency on going from the isolated molecule to $LaF_3 \cdot Ne_2$ complexes because of the steeper curve of LaF_3 at the equilibrium geometry. A similar ν_2 frequency reduction has been previously observed on passing from GdF_3 to $GdF_3 \cdot Ne_2$;[28,29] however, in that case this tendency

TABLE 7: Harmonic Vibrational Frequencies of LnX_3 and $LnX_3 \cdot IG_2$ (IG = Ne, Ar, Xe, and N_2) Systems[a]

	SCF/cm^{-1}				MP2/cm^{-1}				experiment[b]/cm^{-1}			
	ν_1	ν_2	ν_3	ν_4	ν_1	ν_2	ν_3	ν_4	ν_1	ν_2	ν_3	ν_4
LaF_3	523.4	10.0	514.8	125.9	524.3	44.9	516.3	120.9	540 ± 10		510 ± 10	
$LaF_3 \cdot Ne_2$	521.5	24.3	512.9	125.7	517.9	14.1	513.0	120.1	527.9	81	496.6	130
$LaF_3 \cdot Ar_2$	518.8	33.9	510.3	125.3	513.6	23.8	509.4	119.4	513.0	83	479.0	121.2
										(84)	(478)	(120)
$LaF_3 \cdot Xe_2$	515.8	38.1	507.4	124.5	509.6	32.9	505.6	118.2				
$LaF_3 \cdot (N_2)_2$	511.3	48.9	503.1	122.1	507.3	35.0	503.4	117.0	490	94	459	112
										(84)	(457)	(116)
LuF_3	596.0	58.7	584.3	145.8	594.9	20.1	585.2	149.6				
$LuF_3 \cdot Ne_2$	592.5	71.3	580.7	145.3	589.2	50.4	579.3	147.7	585.4	101	570.5	150
$LuF_3 \cdot Ar_2$	588.6	78.6	577.1	144.5	583.2	74.1	573.5	146.7	569.6	112	552.2	144
$LuF_3 \cdot Xe_2$	584.6	78.8	573.2	143.3	577.7	75.0	567.8	144.7				
$LuF_3 \cdot (N_2)_2$	578.6	97.1	567.4	140.2	573.6	90.4	563.5	142.1		121	530	149
$LaCl_3$	305.9	31.8	325.1	71.7	311.8	1.9	337.0	68.8		≈30[c]	317	≈70[c]
$LaCl_3 \cdot Ne_2$	304.3	38.4	323.3	71.7	309.9	30.0	335.0	68.7				
$LaCl_3 \cdot Ar_2$	301.4	44.6	320.3	71.6	306.7	39.4	331.9	68.1				
$LaCl_3 \cdot Xe_2$	298.6	50.0	317.4	70.9	303.7	40.7	328.6	67.6		52	300	74
$LaCl_3 \cdot (N_2)_2$	297.2	50.1	316.2	70.1	303.4	38.4	328.8	66.6				
$LuCl_3$	335.8	54.0	353.4	83.0	341.6	42.1	364.4	80.8				
$LuCl_3 \cdot Ne_2$	333.0	70.3	350.0	83.3	338.8	65.5	360.7	82.3				
$LuCl_3 \cdot Ar_2$	330.4	70.9	347.3	82.7	334.0	78.5	355.6	82.3				
$LuCl_3 \cdot Xe_2$	326.6	69.0	343.5	81.6	330.0	85.0	351.5	80.2		60	331	88
$LuCl_3 \cdot (N_2)_2$	322.4	85.0	338.2	80.2	329.8	84.4	350.9	79.3				

[a] Only intramolecular LnX_3 frequencies are reported. [b] Experimental data are taken from refs 6, 8, 9, 10, 11, and 12. [c] Estimated from Figure 1 in ref 6.

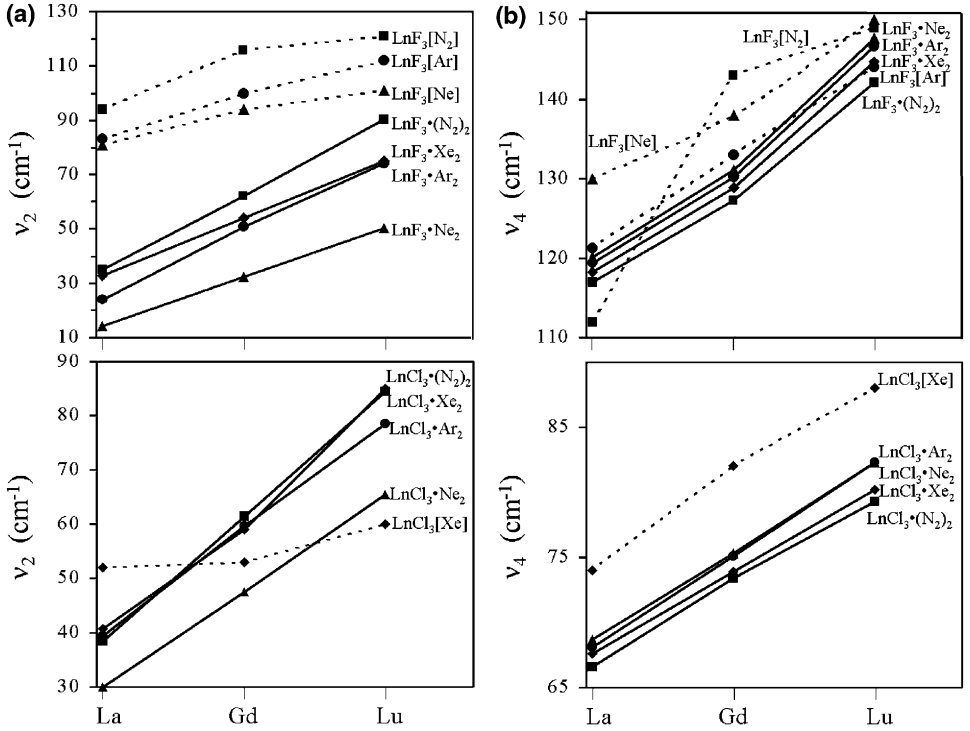

Figure 6. Experimental (LnX_3[IG], dashed lines) and MP2 computed ($LnX_3 \cdot IG_2$, solid lines) frequencies for out-of-plane (left) and in-plane bending (right) for trifluoride and trichloride molecules trapped in inert-gas matrices. Data for $GdX_3 \cdot IG_2$ complexes have been taken from refs 28 and 29.

was less pronounced because of the minor propensity of the GdF_3 molecule to adopt a pyramidal structure.[28,29] A monotonic increase of the out-of-plane bending frequency is observed on going from isolated molecules to inert-gas complexes for all of the other $LnX_3 \cdot IG_2$ species. Figure 6 reports the computed and experimental ν_2 frequency (including previous results on $GdX_3 \cdot IG_2$) for each $LnX_3 \cdot IG_2$ series on increasing lanthanide atomic number (experimental data are indicated as LnX_3[IG]).

For both fluorides and chlorides the ν_2 frequency increases linearly with the atomic number of the lanthanide. The slope is roughly independent of inert-gas matrices while it is steeper for fluorides than for chlorides and the average line fittings are: $\nu_2(LnF_3 \cdot IG_2) = 3.3m + p$; $\nu_2(LnCl_3 \cdot IG_2) = 2.9m + p$, where m represents the position number in the lanthanide series ($m_{La} = 0$, $m_{Gd} = 7$, $m_{Lu} = 14$); the intercept p is the ν_2 frequency of $LaX_3 \cdot IG_2$, and it is characteristic of each series.[52] The computed trend for fluorides is very similar to that deduced from IR measurements of molecules trapped in matrices. Thus, the straight line related to the neon matrix is found at the lowest wavenumbers followed by those obtained for argon, xenon, and finally nitrogen matrices. Also, slopes obtained by fitting the three experimental points are roughly independent of inert-gas matrices, but they are less steep than that computed; the average line fitting is $\nu_2(LnF_3[IG]) = 1.8m + p$. The computed intercept

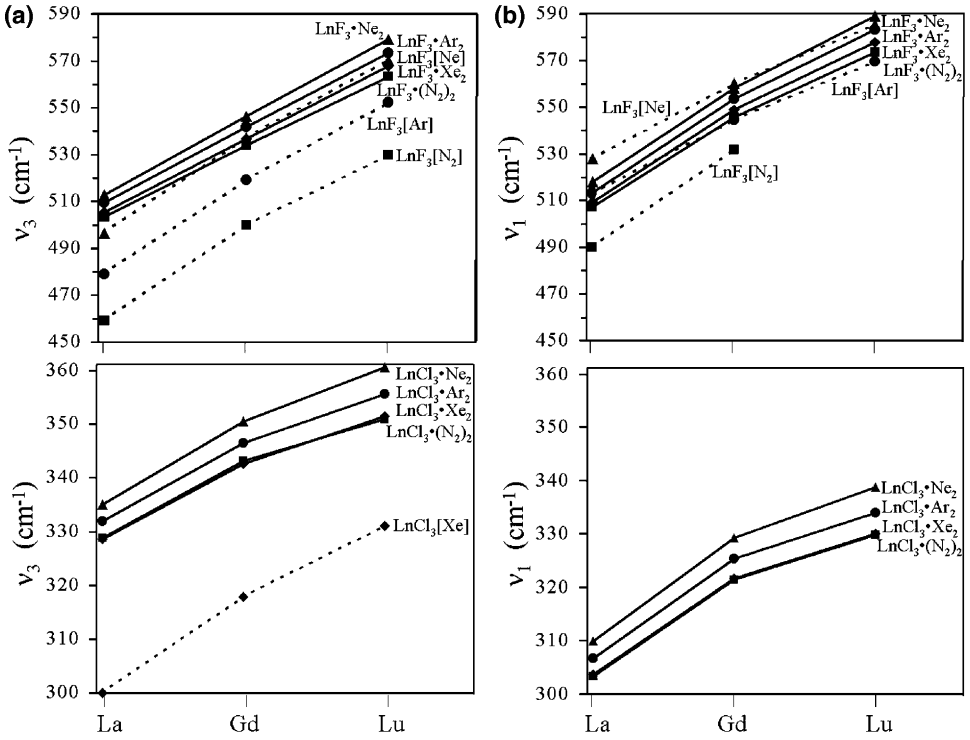

Figure 7. Experimental (LnX_3[IG], dashed lines) and MP2 computed (LnX_3•IG_2, solid lines) frequencies for asymmetric (left) and symmetric (right) stretching for trifluoride and trichloride molecules trapped in inert-gas matrices. Data for GdX_3•IG_2 complexes have been taken from refs 28 and 29.

"*p*" for each LnF_3•IG_2 series differs considerably from that derived from experimental data.[52] Both differences are mainly due to the simplified model we used to simulate matrix effects and clearly indicate that LnF_3 molecules maintain higher flexibility toward the out-of-plane deformation in LnF_3•IG_2 complexes than that found in the real matrix environment. More reliable systems, certainly, would provide a better quantitative comparison even though qualitative trends are well reproduced by the proposed LnF_3•IG_2 model. The only experimental data available for $LnCl_3$ molecules are those obtained in the xenon matrix: $\nu_2(LnCl_3[Xe]) = 0.6m + p$.[9,52] The experimental trend is qualitatively similar to computational data, i.e. the ν_2 frequency increases for heavier lanthanides.

The computed ν_4 scissors-type bending frequency is less sensitive to inert-gas coordination (Table 7, Figure 6). It generally diminishes on passing from gas-phase LnX_3 molecules to LnX_3•IG_2 complexes and on increasing of the LnF_3- - -IG_2 interaction energy. For both fluorides and chlorides the ν_4 frequency increases almost linearly with the atomic number of the lanthanide. The slope is roughly independent of the inert-gas matrices considered (Figure 6), and it is steeper for fluorides than for chlorides: $\nu_4(LnF_3$•$IG_2) = 1.9m + p$; $\nu_4(LnCl_3$•$IG_2) = 0.95m + p$. Excluding experimental data of LnF_3•$[N_2]$ which seem rather irregular, computed trends are in close agreement with those obtained in IR measurements. Thus, the LnF_3•[Ar] curve lies at lower wavenumbers than that obtained for the LnF_3•[Ne] series and the experimentally derived slopes ($\nu_4(LnF_3$•$IG_2) = 1.5m + p$; $\nu_4(LnCl_3$•$IG_2) = 1.0m + p$) are close to those computed for the LnX_3•IG_2 model.

The host matrix affects even stiff stretching modes (Table 7, Figure 7); thus, a consistent reduction of both ν_1 and ν_3 frequency modes is noticed on passing from isolated molecules LnX_3 to inert-gas complexes LnX_3•IG_2 in agreement with the R_{Ln-X} bond weakening discussed above. The reduction is roughly proportional to the interaction energy. Therefore, the frequency shift increases on passing from RHF to MP2 wave functions and across the series LnX_3•Ne_2 < LnX_3•Ar_2 < LnX_3•Xe_2 < LnX_3•$(N_2)_2$. Measured IR frequencies for the $LaCl_3$ molecule trapped in xenon matrix at 20−30 K are reported in Table 7 and compared with $LaCl_3$ gas-phase experimental data (1350 K) and present theoretical results. Going from gas-phase to xenon matrix, experimental ν_3 frequency undergoes a considerable reduction (∼17 cm^{-1}) as qualitatively predicted by calculations on the $LaCl_3$•Xe_2 model complex (8.4 cm^{-1}). These data indicate that the simple $LnCl_3$•Xe_2 model roughly accounts for 50% of total matrix effect on the ν_3 stretching frequencies.

Computational data on LnX_3•IG_2 model complexes (Figure 7) point to a monotonic growth of ν_1 and ν_3 frequencies on increasing the lanthanide atomic number, and the average slopes for fluorides and chlorides are $\nu_1(LnF_3$•$IG_2) = 4.9m + p$; $\nu_3(LnF_3$•$IG_2) = 4.5m + p$; $\nu_1(LnCl_3$•$IG_2) = 1.9m + p$; $\nu_3(LnCl_3$•$IG_2) = 1.7m + p$. The straight lines for all the frequencies are ordered in function of decreasing wavenumbers LnX_3•Ne_2 > LnX_3•Ar_2 > LnX_3•Xe_2 > LnX_3•$(N_2)_2$, and they are steeper for fluorides than for chlorides. These results are borne out in experimental IR measurements of LnX_3[IG]. Thus, the experimental ν_3 and ν_1 straight lines for fluorides follow the order LnF_3[Ne] > LnF_3[Ar] > LnF_3[N_2], and for both the fluoride and chloride series the slopes from theoretical data are close to those derived experimentally: $\nu_1(LnF_3[IG]) = 4.7m + p$; $\nu_3(LnF_3[IG]) = 5.2m + p$; $\nu_3(LnCl_3$•[Xe]) = $1.7m + p$.[52] Furthermore, the computed intercepts "*p*" for the ν_1 vibrational frequency in the LnF_3•IG_2 model series are close to experimental values; thus, theoretical and experimental curves almost overlap.

Conclusions

The recent history of theoretical and experimental studies directed toward elucidating spectroscopic properties of monomeric rare-earth halides demonstrates that the huge mass of the metal, the large metal radius, the availability of orbitals s, p, d,

and f for the formation of bonds give rise to various and surprising features. The high polarizability of semicore orbitals and the presence of low-lying empty orbitals produce very shallow ground-state minima, and the different molecular symmetry and geometrical parameters on comparing equilibrium or vibrational average of structures is not an exception but a rule. In line with this view, spectroscopic parameters, derived for molecules in the gas-phase at high temperature, are generally different from those obtained when molecules are embedded in inert-gas matrices at cryogenic temperatures.

Emerging rigorous computational studies offer a complementary and independent tool to probe the molecular properties of rare-earth halides. For example, present computed anharmonic vibrational frequencies for gas-phase LnX_3 molecules allow a rational and exhaustive interpretation of the high-temperature, gas-phase IR spectrum of $LaCl_3$, while for other molecules, some spectral predictions are reported and invite experimental verification. In any case, generally great care has to be taken in comparing theoretical results and experimental data, since sometimes the corresponding parameters have different meanings as in the case of equilibrium or thermal-average structures. Therefore, throughout appropriate models, anharmonic vibrational effects should be included in computational data to derive thermal-average structures, or they should be subtracted from experimental data to derive equilibrium structures. These analyses would allow a reasonable theoretical/experimental comparison. Furthermore, such molecules might be in different "physical states" such as when they are embedded in inert-gas matrices. Note that the term "inert" is sometime misleading, since host−guest interactions have been found to be substantial, and computed data for $LnX_3 \cdot IG_2$ demonstrate that the "spectroscopic accuracy" can be reached only by including matrix effects.

Appendix

Among the analyzed molecules the spin−orbit coupling should be greater for the $LuCl_3$ due to two independent reasons, (i) the lutetium has a greater atomic number than lanthanum and (ii) the chlorine atoms produce a more covalent molecular environment around the metal with respect to fluorine atoms. Therefore, spin−orbit effects have been explicitly taken into account for $LuCl_3$, and conclusions could be extended to the remaining systems under investigation.

It is appropriate to base spin−orbit calculations on electronic states derived from configuration interaction wave functions. Therefore, preliminary configuration interaction including single and double excitations (CISD) calculations were performed to assess low-lying triplet states and to choose an opportune and computationally feasible window of occupied and empty molecular orbitals for CI expansion. The selected active space for CISD wave functions consists of the Lu_{4f}, Lu_{5d}, Lu_{6s}, Lu_{6p}, Cl_{3s}, and Cl_{3p} valence atomic orbitals (i.e., 38 electrons in 28 orbitals). In the C_1 symmetry they give rise to 14878 and 1687770 configuration state functions for singlet and triplet states, respectively.

The CISD calculations show that there is a manifold of six triplet states, three of which are degenerate, ∼150 kcal/mol above the electronic ground state. These states arise from the excitation of one electron from each valence molecular orbital $(a_1')^2(e')^4(e'')^2(e')^4(a_2'')^2(a_2')^2$ to the LUMO (a_1'). Applying simple symmetry selection rules, it is evident that only the $^3A_2'$ and $^3E''$ states can interact through the spin−orbit Hamiltonian with the $^1A_1'$ ground state in D_{3h} symmetry, while upon bending (C_{3v} symmetry), two additional ^3E states may interact with the $^1A_1$ ground state. The spin−orbit coupling of two different spin states was determined by using the relativistic Breit−Pauli Hamiltonian with both one- and two-electron terms as implemented in the GAMESS code.[34,53−55]

TABLE A: Spin−Orbit Coupling Constants (cm^{-1}) for $LuCl_3$ at Various Bond Angles (R = 2.450 Å)

states[a]	120°	119°
$^3A_2'$ ($^3A_2$)	73.5	60.8
$^3A_2''$ ($^3A_1$)	0.0	0.0
$^3E''$ (^3E)	53.8	50.1
$^3E'$ (^3E)	0.0	11.9
$^3E'$ (^3E)	0.0	9.7
$^3A_1'$ ($^3A_1$)	0.0	0.0

[a] Low-lying triplet states in D_{3h} and C_{3v} (in parentheses) symmetries.

For the planar D_{3h} arrangement, the spin−orbit coupling constants, 73.5 cm^{-1} ($^1A_1'-^3A_2'$) and 53.8 cm^{-1} ($^1A_1'-^3E''$), indicate a small coupling between the ground state and the low-lying triplet states, therefore suggesting a very small perturbation of adiabatic CISD surface around the minimum. In fact, the energy difference between the lowest spin−orbit state and the adiabatic CISD energy amounts to 0.12 cm^{-1}, thus leaving unchanged equilibrium geometrical parameters (R_{Lu-Cl} = 2.450 Å, Θ = 120°). For pyramidal configurations, as expected, there is a greater number of triplet states involved in spin−orbit coupling. Interactions related to the two "new" ^3E states are modest, while those involving $^3A_2$ and ^3E, which correlate with the $^3A_2'$ and $^3E''$ states in D_{3h} symmetry, undergo minor variations, thus leaving unchanged the potential energy surface along the out-of-plane motion (see Table A).

In summary, for the presently analyzed LnX_3 molecules it is more important to address interelectronic repulsions and high-order electronic correlation effects rather than spin−orbit coupling, since the latter effect on geometries is very small.

References and Notes

(1) Hargittai, M. *Chem. Rev.* **2000**, *100*, 2233.
(2) Kovacs, A.; Konings, R. J. M. *J. Phys. Chem. Ref. Data* **2004**, *33*, 377.
(3) Giricheva, N. I.; Zakharov, A. V.; Shlykov, S. A.; Girichev, G. V. *J. Chem. Soc., Dalton Trans.* **2000**, 3401.
(4) Hargittai, M. *J. Phys. Chem. A* **1999**, *103*, 7552.
(5) Réffy, B.; Marsden, C. J.; Hargittai, M. *J. Phys. Chem. A* **2003**, *107*, 1840.
(6) Kovacs, A.; Konings, R. J. M.; Booij, A. S. *Chem. Phys. Lett.* **1997**, 268, 207.
(7) Kovacs, A.; Konings R. J. M.; Booij, A. S. *Vibrat. Spectrosc.* **1995**, *10*, 65.
(8) Selivanov, G. K.; Sekachev, Y. N.; Mal'tsev, A. A. *Russ. J. Phys. Chem.* **1973**, *47*, 1239.
(9) Perov, P. A.; Nedyak S. V.; Mal'tsev, A. A. *Vestn. Mosk. Univ., Ser. 2: Khim.* **1975**, *16*, 281.
(10) Hauge, R. H.; Hastie J. W.; Margrave, J. L. *J. Less-Common Met.* **1971**, *23*, 359.
(11) Hauge, R. H.; Hastie J. W.; Margrave, J. L. *J. Less-Common Met.* **1975**, *39*, 309.
(12) Wesley, R. D.; DeKock, C. W. *J. Chem. Phys.* **1971**, *55*, 3866.
(13) Leisiecki, M.; Nibler, J. W.; DeKock, C. W. *J. Chem. Phys.* **1972**, *57*, 1352.
(14) Ruscic, B.; Goodman, G. L.; Berkowitz, J. *J. Chem. Phys.* **1983**, *78*, 5443.
(15) Beattie, I. R. *Angew. Chem., Int. Ed.* **1999**, *38*, 3294.
(16) Dolg, M.; Stoll, H.; Preuss, H. *J. Mol. Struct. (THEOCHEM)* **1991**, *235*, 67.
(17) Di Bella, S.; Lanza, G.; Fragalà, I. L. *Chem. Phys. Lett.* **1993**, *214*, 598.
(18) Lanza, G.; Fragalà, I. L. *Chem. Phys. Lett.* **1996**, *255*, 341.
(19) Lanza, G.; Fragalà, I. L. *J. Phys. Chem. A* **1998**, *41*, 7995.
(20) Cundari, T. R.; Sommerer, S. O.; Strohecker, L. A.; Tippett, L. *J. Chem. Phys.* **1995**, *103*, 7085.
(21) Adamo C.; Maldivi, P. *J. Phys. Chem. A* **1998**, *102*, 6812.
(22) Adamo C.; Barone, V. *J. Comput. Chem.* **2000**, *21*, 1153.

(23) Joubert, L.; Picard G.; Legendre, J.-J. *J. Alloys Compd.* **1998**, *275*−*277*, 934.
(24) Joubert, L.; Picard, G.; Legendre, J.-J. *Inorg. Chem.* **1998**, *37*, 1984.
(25) Solomonik, V. G.; Marochko, O. Y. *J. Struct. Chem. Engl. Tr.* **2000**, *41*, 725.
(26) Tsuchiya, T.; Taketsugu, T.; Nakano, H.; Hirao, K. *J. Mol. Struct. (THEOCHEM)* **1999**, *461*−*462*, 203.
(27) Jansik, B.; Sanchez de Meras, A. M. J.; Schimmelpfenning, B.; Ågren, H. *J. Chem. Soc., Dalton Trans.* **2002**, 4603.
(28) Lanza, G.; Minichino, C. *ChemPhysChem* **2004**, *5*, 120.
(29) Lanza, G.; Minichino, C. *J. Phys. Chem. A* **2004**, *108*, 4949.
(30) Cundari, T. R.; Stevens, W. J. *J. Chem. Phys.* **1993**, *98*, 5555.
(31) Stevens, W. J.; Krauss, M.; Basch, H.; Jasien, P. G. *Can. J. Chem.* **1992**, *70*, 612.
(32) Dunning, T. H., Jr. *J. Chem. Phys.* **1971**, *55*, 716.
(33) McLean, A. D.; Chandler, G. S. *J. Chem. Phys.* **1980**, *72*, 5639.
(34) Schmidt, M. W.; Baldridge, K. K.; Boatz, J. A.; Elbert, S. T.; Gordon, M. S.; Jensen, J. H.; Koseki, S.; Matsunaga, N.; Nguyen, K. A.; Su, S. J.; Windus, T. L.; Dupuis, M.; Montgomery, J. A. *J. Comput. Chem.* **1993**, *14*, 1347.
(35) Frisch, M. J.; Trucks, G. W.; Schlegel, H. B.; Scuseria, G. E.; Robb, M. A.; Cheeseman, J. R. V.; Zakrzewski, G.; Montgomery, J. A., Jr.; Stratmann, R. E.; Burant, J. C.; Dapprich, S.; Millam, J. M.; Daniels, A. D.; Kudin, K. N.; Strain, M. C.; Farkas, O.; Tomasi, J.; Barone, V.; Cossi, M.; Cammi, R.; Mennucci, B.; Pomelli, C.; Adamo, C.; Clifford, S.; Ochterski, J.; Petersson, G. A.; Ayala, P. Y.; Cui, Q.; Morokuma, K.; Malick, D. K.; Rabuck, A. D.; Raghavachari, K.; Foresman, J. B.; Cioslowski, J.; Ortiz, J. V.; Stefanov, B. B.; Liu, G.; Liashenko, A.; Piskorz, P.; Komaromi, I.; Gomperts, R.; Martin, R. L.; Fox, D. J.; Keith, T.; Al-Laham, M. A.; Peng, C. Y.; Nanayakkara, A.; Gonzalez, C.; Challacombe, M.; Gill, P. M. W.; Johnson, B.; Chen, W.; Wong, M. W.; Andres, J. L.; Gonzalez, C.; Head-Gordon, M.; Replogle, E. S.; Pople, J. A. *Gaussian 98*, revision A.6; Gaussian, Inc.: Pittsburgh, PA, 1998.
(36) Chaban, G. M.; Jung, J. O.; Gerber, R. B. *J. Chem. Phys.* **1999**, *111*, 1823.
(37) Barone, V.; Grand, A.; Minichino, C.; Subra, R. *J. Chem. Phys.* **1993**, *99*, 6787.
(38) Minichino, C.; Barone, V. *J. Chem. Phys.* **1994**, *100*, 3717.
(39) Cotton, F. A.; Wilkinson, G.; Murillo, C. A.; Bochmann, M. *Advanced Inorganic Chemistry*; John Wiley & Sons: New York, 1999.
(40) Herzberg, G. *Molecular Spectra and Molecular Structure II. Infrared and Raman Spectra of Polyatomic Molecules*; Van Nostrand Reinhold: New York, 1950.
(41) Bunker, P. R.; Jensen, P. *Molecular Symmetry and Spectroscopy*; NRC Research Press: Ottawa, Canada, 1998; p 496.
(42) Yamada, C.; Hirota, E. *Phys. Rev. Lett.* **1986**, *56*, 923.
(43) Kydd, R. A.; Krueger, P. J. *J. Chem. Phys.* **1978**, *69*, 827.
(44) Judge, R. H.; Moule, D. C. *J. Chem. Phys.* **1983**, *78*, 4806.
(45) Moule, D. C.; Subramaniam, C. R. *J. Chem. Soc. D* **1969**, 1340.
(46) Fischer, G. *J. Mol. Spectrosc.* **1969**, *29*, 37.
(47) Cyvin, S. J. *Molecular Vibrations and Mean Square Amplitude*; Elsevier Publishing Company: Amsterdam, 1968.
(48) Barone, V.; Minichino, C. *J. Mol. Struct.* (*THEOCHEM*) **1995**, *330*, 365.
(49) Akishin, P. A.; Naumor, V. A. *Nauchn. Dokl. Vyssh. Shk. Khim. Khim. Tekhnol.* **1959**, *1*, 5.
(50) Kaupp, M.; Schleyer, P. v. R.; Stoll, H. *J. Phys. Chem.* **1992**, *96*, 9801.
(51) Bihary, Z.; Chaban, G. M.; Gerber, R. B. *J. Chem. Phys.* **2002**, *116*, 5521.
(52) Myers, C. E.; Graves, D. T. *J. Chem. Eng. Data* **1977**, *22*, 436.
(53) Furlani, T. F.; King, H. F. *J. Chem. Phys.* **1985**, *82*, 5577.
(54) King, H. F.; Furlani, T. F. *J. Comput. Chem.* **1988**, *9*, 771.
(55) Fedorov, D. G.; Gordon, M. S. *J. Chem. Phys.* **2000**, *112*, 5611.